

Tunable Spectral Ordering of Magnetic Plasmons

Nicholas P. Montoni, Steven C. Quillin, Charles Cherqui, and David J. Masiello*

Department of Chemistry, University of Washington, Seattle, WA 98195

E-mail: masiello@chem.washington.edu

Abstract

Ring-like assemblies of metal nanoparticles that exhibit magnetic resonances, called magnetic plasmon oligomers, have been of recent interest as negative-index metamaterials and light-harvesting devices. For these reasons, it is imperative to understand the properties of such systems on the single- to few-oligomer scale. We show through theory and simulation that the energy ordering of the magnetic resonances of few-oligomer systems depends on size, scale, and environment in ways that purely electric plasmons do not. We show that the dynamic ordering of the eigenmodes of magnetic systems is due entirely to retardation effects and can be understood by inspecting the intermediate- and far-field contributions which are excluded in the quasistatic approximation. We highlight the versatility and tunability of magnetic plasmon oligomers, elucidating a previously unexplored physical phenomenon and suggesting future applications of magnetic plasmons in highly sensitive detection methods.

Keywords

plasmon, hybridization, magnetic, retardation

1 Introduction

Metal nanoparticles (MNPs) support collective resonances of their conduction electrons at optical frequencies. These localized surface plasmon resonances (LSPRs) can interact with each other in assemblies to produce hybridized resonances, much like the hybridization of atomic orbitals in molecules.^{1–4} When these MNPs are arranged in rings, the single LSPRs can give rise to a collective mode that produces an oscillating magnetic dipole in the center of the ring.^{5–10} Such systems are known as magnetic plasmon oligomers and have been of intense focus due to their potential applications in sensing,^{11–18} lensing,^{19,20} cloaking,²¹ and information processing.^{22–24} In Cherqui’s 2014 work on magnetic plasmons, a quasistatic, electric dipole tight-binding model was used to describe the magnetic systems;⁹ we adapt this model to expand on the results of that work. Cherqui’s model considered only the electric near-field of the single-particle plasmons and only incorporated nearest-neighbor interactions. As a result, while it accurately predicted the magnetic eigenmodes, it inaccurately described their energy ordering as confirmed by simulation. An explanation was needed to determine why the tight-binding model would predict different energy-ordering than full-wave simulations.

In a recent paper, Engheta *et al.* state that magnetic systems are well-understood on the single oligomer scale and the nearly infinite scale.²⁵ Furthermore, the dependence of magnetic properties on individual nanoparticle geometry and the relative size of the constituent oligomers has also been determined.¹⁰ However, the properties of few-oligomer systems have not been fully explored. Here we show that to fully understand the properties of magnetic oligomers on the few-oligomer scale, the simple tight-binding model described above must be extended to include both the fully-retarded electric fields and all inter-particle interactions. We show this through three explorations of oligomer properties: system size, dielectric constant of the environment, and inter-particle spacing, and we confirm our results using full-wave simulations.²⁶

It is well-known that as MNPs and aggregates become larger, the quasistatic approximation breaks down. There has been much work done to elucidate the effects of retardation on

large MNPs,^{27,28} dimers,^{29–31} and extended chains and 2-D arrays of particles.^{32–35} Magnetic oligomers composed of two or more rings of particles have the potential to be hundreds of nanometers to microns across, justifying the need to consider retardation effects in determining their optical properties. In order to incorporate retardation effects into quasistatic plasmon hybridization theory, we begin by mapping the dipole plasmon of each MNP onto a set of harmonic oscillators, and allow them to couple through their electric fields according to the following Hamiltonian:⁹

$$H = \sum_i^n \frac{\mathbf{P}_i^2}{2m_{\text{sp},i}} + \frac{1}{2} m_{\text{sp},i} \omega_{\text{sp},i}^2 \mathbf{X}_i^2 - e^2 \sum_{i>j} \mathbf{X}_i \cdot \boldsymbol{\Lambda}_{ij} \cdot \mathbf{X}_j, \quad (1)$$

where \mathbf{P}_i are the momenta conjugate to the plasmon coordinates \mathbf{X}_i , $\omega_{\text{sp},i}$ are the individual LSPR frequencies of each oscillator, $m_{\text{sp},i}$ are the LSPR effective masses and $\boldsymbol{\Lambda}_{ij}$ is the fully retarded dipole-dipole relay tensor (expanded below).³⁶ To make this Hamiltonian more manageable, it is nondimensionalized using $\mathbf{Q}_i = (m_{\text{sp}} \omega_{\text{sp}} / \hbar)^{\frac{1}{2}} \mathbf{X}_i$ and $\boldsymbol{\Pi}_i = \mathbf{P}_i / \sqrt{\hbar m_{\text{sp}} \omega_{\text{sp}}}$. Substituting into Equation 1 and expanding $\boldsymbol{\Lambda}_{ij}$, we get:

$$\begin{aligned} H = & \frac{\hbar \omega_{\text{sp}}}{2} \sum_i^n [\boldsymbol{\Pi}_i^2 + \mathbf{Q}_i^2] - \frac{\hbar \omega_{\text{sp}}}{2\varepsilon_b} \sum_{i>j} \{ g_{ij}^{\text{NF}} [3(\mathbf{Q}_i \cdot \hat{\mathbf{n}}_{ij})(\hat{\mathbf{n}}_{ij} \cdot \mathbf{Q}_j) - \mathbf{Q}_i \cdot \mathbf{Q}_j] \\ & + g_{ij}^{\text{IF}} [3(\mathbf{Q}_i \cdot \hat{\mathbf{n}}_{ij})(\hat{\mathbf{n}}_{ij} \cdot \mathbf{Q}_j) - \mathbf{Q}_i \cdot \mathbf{Q}_j] \\ & - g_{ij}^{\text{FF}} [(\mathbf{Q}_i \cdot \hat{\mathbf{n}}_{ij})(\hat{\mathbf{n}}_{ij} \cdot \mathbf{Q}_j) - \mathbf{Q}_i \cdot \mathbf{Q}_j] \}, \end{aligned} \quad (2)$$

In this Hamiltonian we introduce the near, intermediate, and far-field coupling terms: $g_{ij}^{\text{NF}} = \frac{\alpha'_{\text{sp}}}{r_{ij}^3} \cos(kr_{ij})$, $g_{ij}^{\text{IF}} = \frac{\alpha'_{\text{sp}} k}{r_{ij}^2} \sin(kr_{ij})$, and $g_{ij}^{\text{FF}} = \frac{\alpha'_{\text{sp}} k^2}{r_{ij}} \cos(kr_{ij})$, respectively, with wavenumber $k = \sqrt{\varepsilon_b \omega_c}$. Additionally, r_{ij} is the distance between the i th and j th LSPRs and $\hat{\mathbf{n}}_{ij}$ is the unit vector connecting two LSPRs. We further incorporate retardation effects by considering the lattice dispersion in the polarizability $\alpha'_{\text{sp}} = (\alpha_{\text{sp}}^{-1} - i \frac{2}{3} k^3)^{-1}$ with $\alpha_{\text{sp}} = r_0^3 \frac{3}{\varepsilon_\infty - 2\varepsilon_b}$. Including these terms, we have incorporated all retardation effects associated with point dipoles.^{37,38}

It should be noted that this Hamiltonian, when diagonalized, results in a transcendental

equation whose solutions, the eigenvalues ω , are functions of themselves. In order to fully solve this problem, we make a first guess of ω for a particular mode of interest and iteratively compute the eigenvalues. Using the eigenvalue associated with the mode of interest, the Hamiltonian is diagonalized to convergence. The process is repeated for each mode of interest.

2 Results and Discussion

In this work, we model silver nanoparticles using a Drude model with $\omega_p = 9.1$ eV, $\varepsilon_\infty = 3.77$, and $\gamma = 0.003$ eV. Note that we have greatly reduced the damping constant in order to better resolve the magnetic modes in the simulations. The oligomer unit cell is a six-member ring, with silver nanoparticles located at the vertices of a regular hexagon. We explore and manipulate three magnetic oligomer systems: a twomer, a linear threemer, and a triangular threemer. The number of rings in a magnetic system corresponds to the number of magnetic modes in the system.⁹ The twomer supports an in-phase mode (North-North, or NN) and an out-of-phase mode (North-South, or NS). The linear threemer supports an all in-phase mode (All-North, or AN), a minimally out-of-phase mode (North-South, or NS), and a maximally out-of-phase mode (North-South-North, or NSN). The triangular threemer supports an all in-phase mode (All-North, or AN) and two degenerate out-of-phase modes (North-South, or NS). These modes and their relative magnetic fields are depicted in Figures 1, 4, and 5. In each exploration, the particles have radius r_0 and nearest-neighbor spacing r_{nn} . In the first set of model calculations, we compare to full-wave simulations to verify that the model accurately captures the properties of the systems, but beyond that we cease comparison to simulation in order to focus on the predictive power of the model. The first calculations, depicted in Figure 1 show how the magnetic modes of the twomer and threemers are impacted by the overall scale of the system. In these calculations, the nearest neighbor distances are held at $r_{nn} = 3 \times r_0$ while r_0 varies from 1 nm to 30 nm.

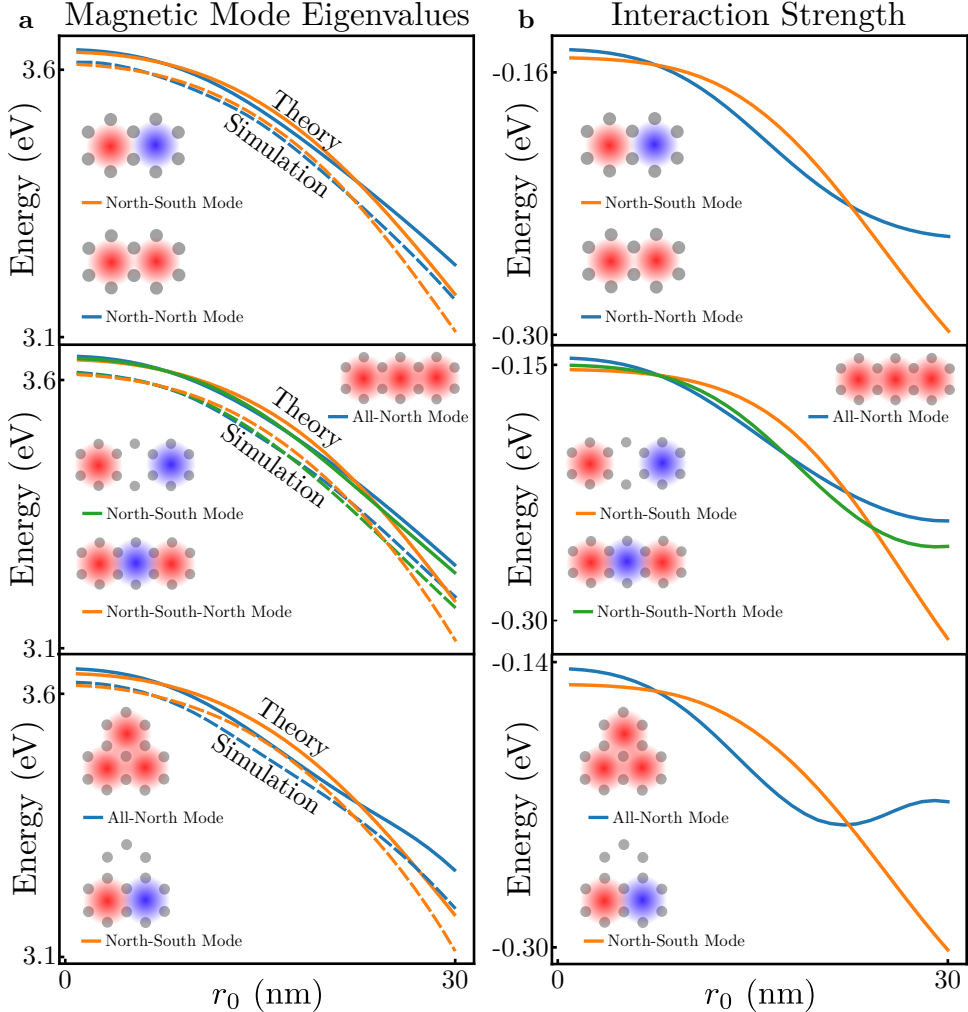


Figure 1: Magnetic mode eigenvalues (column a), predicted and simulated, and interaction strengths (column b) for the magnetic twomer (first row), linear threemer (second row), and triangular threemer (third row). All of the magnetic modes range from 3.1 eV to 3.6 eV. In each system, the magnetic modes exhibit multiple crossings, showing that the eigenspectrum of these magnetic systems depends on their scale. The model consistently overestimates the eigenvalues by 0.05 eV, and consistently underestimates the crossing points by less than a nanometer. To further emphasize the impact of scale, we have plotted the total interaction strength of each eigenmode, *i.e.* the sum of each eigenvector's dot product with the electric field of all of the other dipoles. This calculation reaffirms the scale-dependence and predicts the same mode crossings as both the eigenvalue calculation and the simulations.

In Figure 1a, the magnetic mode eigenvalues are computed for each system. The solid lines depict model calculations, and the dashed lines depict simulated results. Interestingly, the magnetic modes exhibit a dynamic energy ordering, switching order twice as a function of scale. It is presumable that they continue to flip at larger and larger sizes. This is confirmed by simulations, with the model overestimating the eigenvalues by about 0.05 eV and underestimating the crossing points by under a nanometer. These small errors are consistent across all three systems. Figure 1b displays the computed interaction strength for each eigenmode produced by the tight-binding model,

$$U_{\text{int}} = - \sum_{i>j} \mathbf{p}_i \cdot \boldsymbol{\Lambda}_{ij} \cdot \mathbf{p}_j \quad (3)$$

where \mathbf{p}_i is an eigenvector and $\boldsymbol{\Lambda}_{ij}$ is the dipole relay tensor connecting all of the electric dipoles. This calculation serves as a further confirmation of the mode-switching, as the interaction strengths follow the eigenvalues.

To gain a more complete understanding of why mode-switching does occur in magnetic systems, we compute not only the total interaction strength for the electric plasmons of each magnetic mode, but we break that calculation into its near-, intermediate-, and far-field components. The results of this calculation are displayed in Figure 2. This exploration shows definitively that the near- and intermediate-field terms contribute a total shift of the interaction strength, but the far-field term alone contributes to the mode switching. This can be seen quite clearly in the dipole relay tensors for the near- and intermediate-field,

$$\boldsymbol{\Lambda}_{ij}^{\text{NF,IF}} = 3\hat{\mathbf{n}}_{ij}\hat{\mathbf{n}}_{ij} - \mathbf{1} \quad (4)$$

and the far-field,

$$\boldsymbol{\Lambda}_{ij}^{\text{FF}} = \mathbf{1} - \hat{\mathbf{n}}_{ij}\hat{\mathbf{n}}_{ij} \quad (5)$$

where $\mathbf{1}$ is the unit dyad. Looking at Equations 4 and 5, we see that the ordering of the

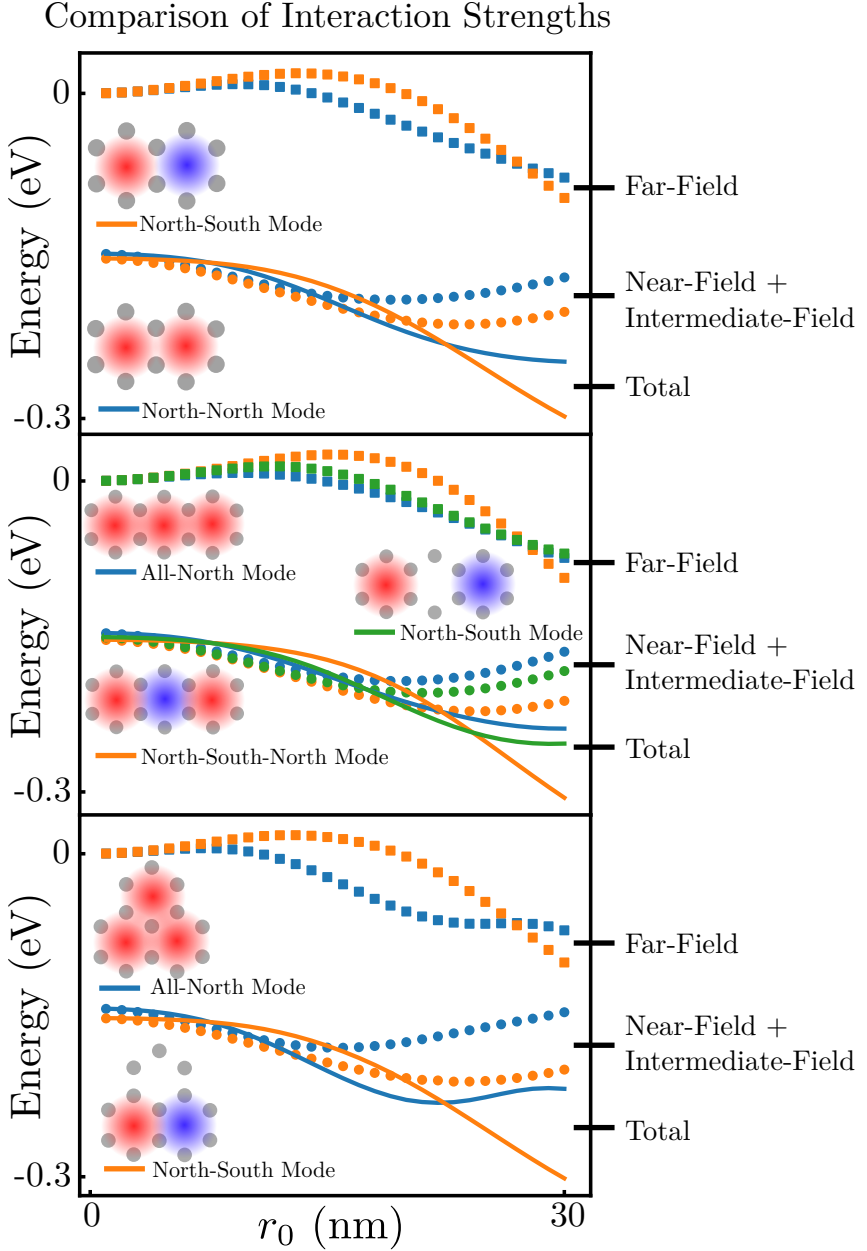


Figure 2: Interactions strengths for the magnetic modes of the twomer (first row), linear threemer (second row), and triangular threemer (third row). We plot as a function of scaling the total interaction strength between the electric plasmons (solid line), the near-field and intermediate-field interaction strength summed (circles), and the far-field interaction strength (squares). In all three systems, the total interaction strengths are the same as those in Figure 1 and so exhibit two mode crossings. The near- and intermediate- fields do not exhibit any crossings at all, and the interaction strengths for each mode simply diverge more and more with greater scaling. The far-field terms do exhibit one crossing towards the larger end of the scaling spectrum, and it is this interplay of far-field with near- and intermediate-field interactions that causes the mode-switching in these magnetic systems.

terms is switched. The form of Equation 4 shows that linearly oriented dipoles contribute more to the interaction energy than parallel dipoles. However, Equation 5 has no contribution from pairs of linearly oriented dipoles and only has equal and opposite contributions from pairs of parallel dipoles [**should I cite the JPCC Steve wrote? Lots about ordering and arrangements of dipoles...**]. Furthermore, the difference in sign on the two dyadic terms in the dipole relay tensors implies that the contributions to the interaction energy from those terms will be of opposite sign for the same pairs of dipoles. The distance-dependence of each field term for different pairs of dipoles is further outlined in Figure 3. The opposition of signs, as well as the crossing in the far-field interaction term, are enough to explain the phenomenon of mode-switching in magnetic oligomers.

We have convinced ourselves that 1) the quasistatic, nearest-neighbors tight-binding model does not contain enough information to agree with fully retarded electrodynamics simulations, 2) those same simulations conform to the results from an updated tight-binding model that incorporates retardation effects and all-particle interactions and 3) the unexpected mode switching exhibited by these magnetic systems is entirely physical and explicable by the varying, distance-dependent decay and oscillation of the electric field terms. With a working model and a basic physical understanding of these three systems, we now perform a series of computations to look at its tunable properties. In the previous section, the scale of the systems was changed. However, this would be impossible to manipulate in a laboratory. We focus on properties with experimental analogues, namely, the dielectric constant of the embedding medium and the nearest-neighbor spacing between nanoparticles.

In order to justify the next set of model calculations, we refer to research on flowing liquid crystal over MNP aggregates and, in real-time, adjusting the refractive index of the MNP environment, influencing the resonance frequencies of the system.³⁹ We apply this concept to our tight-binding model to determine if this has any implications on the properties of magnetic oligomers. What we find is that, as expected, increasing the real-valued dielectric constant of the background decreases the resonance frequency of the collective modes. Fur-

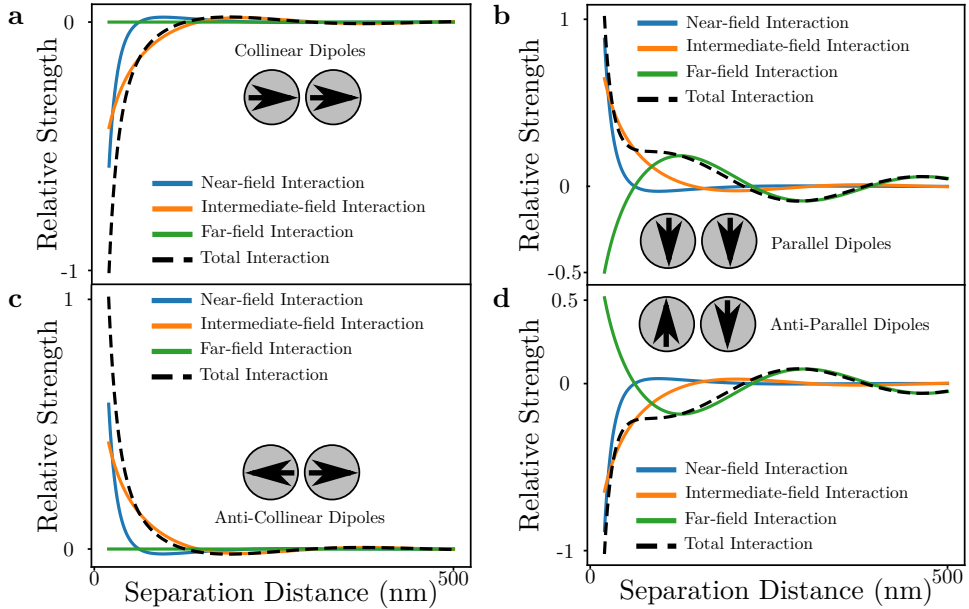


Figure 3: Relative interaction strengths for the four possible dipole arrangements of a nanoparticle dimer: collinear (a), parallel (b), anti-collinear (c), and anti-parallel (d). Plotted are the near-field (blue), intermediate-field (orange), far-field (green), and total (black, dashed) interaction strengths for each set of dipoles as a function of dipole-dipole distance. Interestingly, and stemming from the form of the dipole relay tensor, the far-field interaction term is zero for both pairs of linear dipoles. From these plots, it can be seen that the favorability of a specific dipole arrangement depends on the separation between the dipoles. This can be seen in the fact that each part of the field depends differently on the separation, and each field term contains an oscillating term. At short length scales, the interaction is dominated by the near-field. However, as the distance increases, the interaction is dominated by the intermediate field (a and c) or the far-field (b and d). As a result, there are separation distances at which normally unfavorable arrangements become favorable. Since magnetic oligomers can be described through pairwise interactions of electric dipoles, it follows that the eigenvalues must also change order as different arrangements of electric dipoles become more and less favorable.

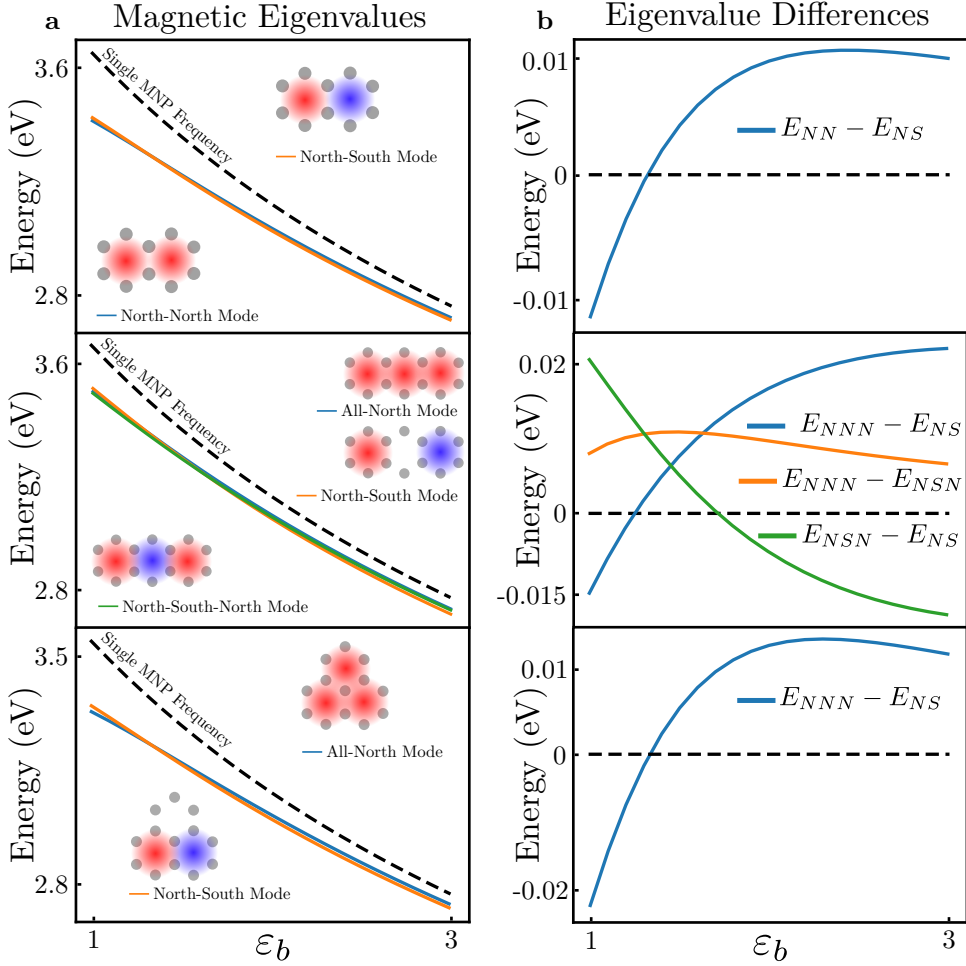


Figure 4: Magnetic mode eigenvalues (column a) for the twomer (first row), linear threemer (second row), and triangular threemer (third row) with particle sizes of 20 nm and magnetic mode eigenvalue differences (column b) as a function of the dielectric constant of an embedding medium. As the dielectric constant is increased from 1 to 3, the magnetic mode splitting approaches zero and the overall energy decreases. At very high dielectric values, the magnetic mode eigenvalues converge to the single particle resonance frequency. This is the result of the dielectric constant reducing the inter-particle interactions. It is also important to note that between $\varepsilon_b = 1$ and $\varepsilon_b = 1.5$, the magnetic mode differences vary sharply, either becoming much more positive or much more negative. This is indicative of mode-switching that is difficult to see in the eigenvalue plots. The increasing dielectric constant has a similar effect to increasing the scale of the system, as it recovers the same energy ordering for $r_0 > 20$ nm.

thermore, the embedding medium influences the energy-ordering of the eigenvalues. Results of one of our explorations are summarized in Figure 4. As the dielectric constant of the medium increases, the eigenmodes collapse onto each other, and eventually converge with the single-particle frequency. Because the modes collapse so quickly and appear to overlap at all values of ε_b , Figure 4b displays the difference in energy between all of the eigenmodes of each system. The values of ε_b where the differences cross zero signify mode-crossing. From these two observations we conclude that increasing the dielectric constant of the embedding medium weakens the overall inter-particle interactions. However, this occurs differently for each of the parts of the interaction. All of the field terms contain similar k -dependence through α'_{sp} and the trigonometric terms, but focusing on how each term depends differently on k in the numerator of the coupling constants (Equation 2) reveals how the dielectric constant influences the electric field. The near-field term contains no other k -dependence, and so is reduced by one factor of ε_b . The intermediate-field term is linear in k , so it is reduced by a factor of $\sqrt{\varepsilon_b}$. Lastly, the far-field term is quadratic in k , so all ε_b -dependence is removed, besides that dependence previously mentioned. At higher values of the dielectric constant the far-field term dominates, much like the way particles that are far apart interact primarily through their far-fields (Figure 3b and d). In other words, embedding magnetic systems in some dielectric medium causes them to act as though they are larger, effectively increasing their scale. This insight provides an experimental route to directly choosing the energy-ordering of magnetic modes, but the reduced splitting between modes might make such an experiment infeasible.

There is also active research on tuning the size and shape of a plasmonic aggregate using various polymers⁴⁰ or DNA.^{41,42} Here, we implement the idea of continuously distorting the nearest-neighbor spacing, from touching to tens of radii apart. We present data for particle radii of 15 nm and 30 nm in Figure 5a and b, respectively. The results of these model calculations are reminiscent of the results in Figure 3 in that the eigenmodes oscillate about each other as the particles move farther apart. In addition, similarly to Figure 4,

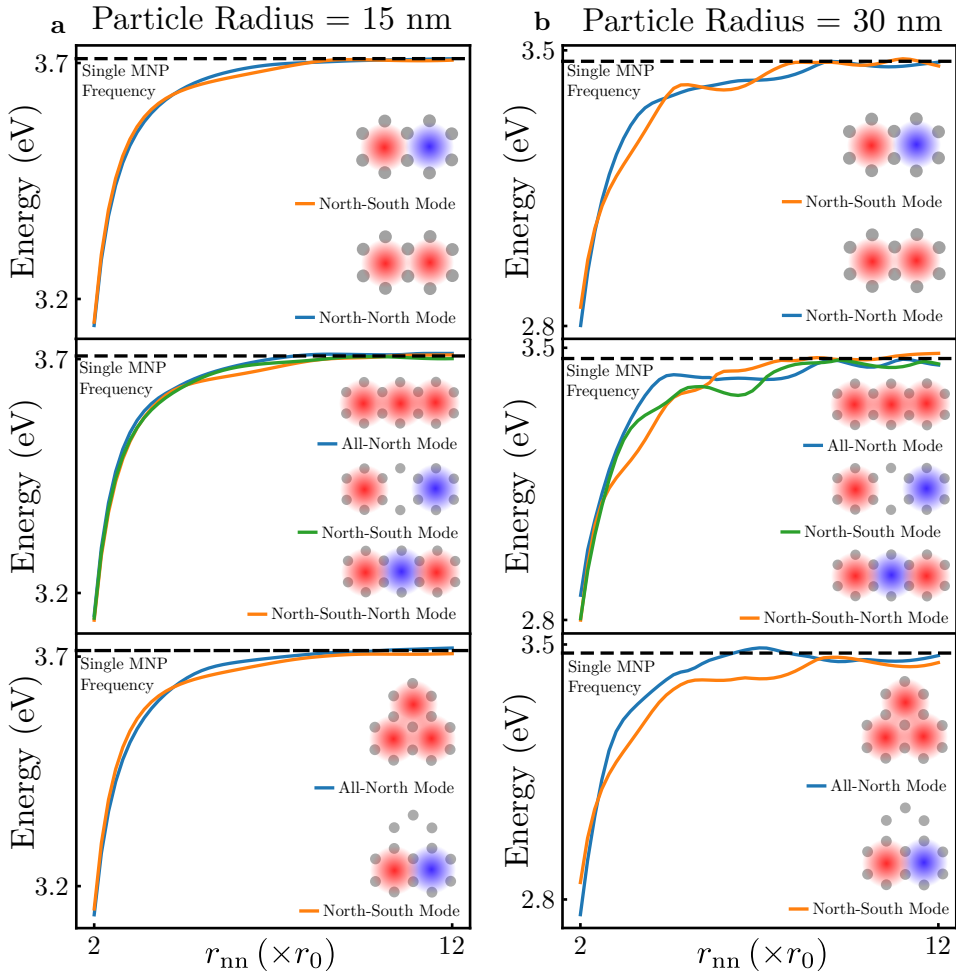


Figure 5: Magnetic mode eigenvalues for the twomer (first row), linear threemer (second row), and triangular threemer (third row) with particle sizes of 15 nm (column a) and 30 nm (column b) as a function of nearest neighbor particle separation in units of radii. As the separation distance increases, the magnetic mode eigenvalues converge to and oscillate about the single particle frequency, exhibiting multiple crossings. As in Equation 2, the interaction strength decays with increasing separation and oscillates due to its dependence on trigonometric functions.

at very large distances the eigenvalues converge to the single LSPR frequency, exhibiting small amplitude oscillations. This is indicative of the coupling falling very near to zero. It is clear that this method, as opposed to the method of tuning the dielectric constant of the background, offers a much greater degree of tunability. Designing a system in which the inter-particle spacing could be varied in discrete steps would lead to the ability to directly choose the resonance frequency of a specific magnetic mode. Furthermore, being able to directly detect the frequency of the magnetic mode optically could turn such magnetic systems into thermometers, pH probes, or detectors of any environmental factor that would change the size of the embedding polymer.

3 Conclusion

We have shown that magnetic systems composed on the few-oligomer scale exhibit tunable resonances with dynamic spectral ordering. However, we stress that the systems studied in this work were chosen due to their theoretical simplicity. In simulated and experimental spectroscopies, these eigenmodes would overlap and be nearly indistinguishable. It has been shown that oligomers whose constituents are rod-like, elongated, or generally degeneracy-breaking have sharper, more isolated magnetic resonances.¹⁰ To this end, future studies will involve these geometries to determine if they have the same eigenmode-switching properties and tunability. With this groundwork on the properties of small oligomers, there is now an incentive and an avenue to expanding the concepts presented here to larger aggregates, as well as a need to confirm the predictions made here with experiments. The ability of the researcher to decide the resonance frequency of a particular eigenmode opens the door to the ability to dynamically and actively determine system properties.

Acknowledgement

CEI, NSF, DOE?, Niket, some other people, probably, HPC.

References

- (1) Clippe, P.; Evrard, R.; Lucas, A. A. Aggregation Effect on the Infrared Absorption Spectrum of Small Ionic Crystals. *Phys. Rev. B* **1976**, *14*, 1715–1721.
- (2) Aravind, P.; Nitzan, A.; Metiu, H. The Interaction between Electromagnetic Resonances and its Role in Spectroscopic Studies of Molecules Adsorbed on Colloidal Particles or Metal Spheres. *Surf. Sci.* **1981**, *110*, 189 – 204.
- (3) Xu, Y. Electromagnetic Scattering by an Aggregate of Spheres. *Appl. Opt.* **1995**, *34*, 4573–4588.
- (4) Mishchenko, M. I.; Mackowski, D. W.; Travis, L. D. Scattering of Light by Bispheres with Touching and Separated Components. *Appl. Opt.* **1995**, *34*, 4589–4599.
- (5) Alù, A.; Salandrino, A.; Engheta, N. Negative Effective Permeability and Left-Handed Materials at Optical Frequencies. *Opt. Express* **2006**, *14*, 1557–1567.
- (6) Alù, A.; Engheta, N. Dynamical Theory of Artificial Optical Magnetism Produced by Rings of Plasmonic Nanoparticles. *Phys. Rev. B* **2008**, *78*, 085112.
- (7) Hentschel, M.; Dregely, D.; Vogelgesang, R.; Giessen, H.; Liu, N. Plasmonic Oligomers: The Role of Individual Particles in Collective Behavior. *ACS Nano* **2011**, *5*, 2042–2050, PMID: 21344858.
- (8) Brandl, D. W.; Mirin, N. A.; Nordlander, P. Plasmon Modes of Nanosphere Trimers and Quadruplets. *J. Phys. Chem. B* **2006**, *110*, 12302–12310.
- (9) Cherqui, C.; Bigelow, N. W.; Vaschillo, A.; Goldwyn, H.; Masiello, D. J. Combined Tight-Binding and Numerical Electrodynamics Understanding of the STEM/EELS Magneto-Optical Responses of Aromatic Plasmon-Supporting Metal Oligomers. *ACS Photonics* **2014**, *1*, 1013–1024.

- (10) Cherqui, C.; Wu, Y.; Li, G.; Quillin, S. C.; Busche, J. A.; Thakkar, N.; West, C. A.; Montoni, N. P.; Rack, P. D.; Camden, J. P. .; Masiello, D. J. STEM/EELS Imaging of Magnetic Hybridization in Symmetric and Symmetry-Broken Plasmon Oligomer Dimers and All-Magnetic Fano Interference. *Nano Lett.* **2016**, *16*, 6668–6676, PMID: 27673696.
- (11) Karaveli, S.; Zia, R. Strong Enhancement of Magnetic Dipole Emission in a Multilevel Electronic System. *Opt. Lett.* **2010**, *35*, 3318–3320.
- (12) Noginova, N.; Zhu, G.; Mavy, M.; Noginov, M. Magnetic Dipole Based Systems for Probing Optical Magnetism. *J. Appl. Phys.* **2008**, *103*, 07E901.
- (13) Wang, J.; Fan, C.; He, J.; Ding, P.; Liang, E.; Xue, Q. Double Fano Resonances Due to Interplay of Electric and Magnetic Plasmon Modes in Planar Plasmonic Structure with High Sensing Sensitivity. *Opt. Express* **2013**, *21*, 2236–2244.
- (14) Zhu, Z.; Bai, B.; You, O.; Li, Q.; Fan, S. Fano Resonance Boosted Cascaded Optical Field Enhancement in a Plasmonic Nanoparticle-in-Cavity Nanoantenna Array and its SERS Application. *Light: Science and Applications* **2015**, *4*, e296.
- (15) Lee, K.-L.; Huang, J.-B.; Chang, J.-W.; Wu, S.-H.; Wei, P.-K. Ultrasensitive Biosensors Using Enhanced Fano Resonances in Capped Gold Nanoslit Arrays. *Scientific Reports* **2015**, *5*, 8547.
- (16) Wu, C.; Khanikaev, A. B.; Adato, R.; Arju, N.; Yanik, A. A.; Altug, H.; Shvets, G. Fano-Resonant Asymmetric Metamaterials for Ultrasensitive Spectroscopy and Identification of Molecular Monolayers. *Nat. Mat.* **2012**, *11*, 69–75.
- (17) Cetin, A. E.; Altug, H. Fano Resonant Ring/Disk Plasmonic Nanocavities on Conducting Substrates for Advanced Biosensing. *ACS Nano* **2012**, *6*, 9989–9995.

- (18) Zhang, S.; Bao, K.; Halas, N. J.; Xu, H.; Nordlander, P. Substrate-Induced Fano Resonances of a Plasmonic Nanocube: a Route to Increased-Sensitivity Localized Surface Plasmon Resonance Sensors Revealed. *Nano Lett.* **2011**, *11*, 1657–1663.
- (19) Fang, N.; Lee, H.; Sun, C.; Zhang, X. Sub-Diffraction-Limited Optical Imaging with a Silver Superlens. *Science* **2005**, *308*, 534–537.
- (20) Valentine, J.; Zhang, S.; Zentgraf, T.; Ulin-Avila, E.; Genov, D. A.; Bartal, G.; Zhang, X. Three-dimensional optical metamaterial with a negative refractive index. *Nature* **2008**, *455*, 376–379.
- (21) Shalaev, V. M. Transforming Light. *Science* **2008**, *322*, 376–379.
- (22) Liu, H.; Genov, D. A.; Wu, D. M.; Liu, Y. M.; Steele, J. M.; Sun, C.; Zhu, S. N.; Zhang, X. Magnetic Plasmon Propagation Along a Chain of Connected Subwavelength Resonators at Infrared Frequencies. *Phys. Rev. Lett.* **2006**, *97*, 243902.
- (23) Liu, N.; Mukherjee, S.; Bao, K.; Brown, L. V.; Dorfmüller, J.; Nordlander, P.; Halas, N. J. Magnetic Plasmon Formation and Propagation in Artificial Aromatic Molecules. *Nano Lett.* **2011**, *12*, 364–369.
- (24) Liu, N.; Mukherjee, S.; Bao, K.; Li, Y.; Brown, L. V.; Nordlander, P.; Halas, N. J. Manipulating Magnetic Plasmon Propagation in Metallic Nanocluster Networks. *ACS Nano* **2012**, *6*, 5482–5488.
- (25) Greybush, N. J.; Liberal, I. n.; Malassis, L.; Kikkawa, J. M.; Engheta, N.; Murray, C. B.; Kagan, C. R. Plasmon Resonances in Self-Assembled Two-Dimensional Au Nanocrystal Metamolecules. *ACS Nano* **2017**, *11*, 2917–2927, PMID: 28190335.
- (26) Hohenester, U.; Trügler, A. MNPBEM - A Matlab Toolbox for the Simulation of Plasmonic Nanoparticles. *Comp. Phys. Comm.* **2012**, *183*, 370 – 381.

- (27) Myroshnychenko, V.; Rodriguez-Fernandez, J.; Pastoriza-Santos, I.; Funston, A. M.; Novo, C.; Mulvaney, P.; Liz-Marzan, L. M.; Garcia de Abajo, F. J. Modelling the optical response of gold nanoparticles. *Chem. Soc. Rev.* **2008**, *37*, 1792–1805.
- (28) Turner, M. D.; Hossain, M. M.; Gu, M. The Effects of Retardation on Plasmon Hybridization within Metallic Nanostructures. *New J. of Phys.* **2010**, *12*, 083062.
- (29) Dahmen, C.; Schmidt, B.; von Plessen, G. Radiation Damping in Metal Nanoparticle Pairs. *Nano Lett.* **2007**, *7*, 318–322, PMID: 17243751.
- (30) Rechberger, W.; Hohenau, A.; Leitner, A.; Krenn, J.; Lamprecht, B.; Aussenegg, F. Optical Properties of Two Interacting Gold Nanoparticles. *Opt. Commun.* **2003**, *220*, 137 – 141.
- (31) Kottmann, J. P.; Martin, O. J. F. Retardation-Induced plasmon Resonances in Coupled Nanoparticles. *Opt. Lett.* **2001**, 1096–1098.
- (32) Haynes, C. L.; McFarland, A. D.; Zhao, L.; Van Duyne, R. P.; Schatz, G. C.; Gunnarsson, L.; Prikulis, J.; Kasemo, B.; Käll, M. Nanoparticle Optics: The Importance of Radiative Dipole Coupling in Two-Dimensional Nanoparticle Arrays. *J. Phys. Chem. B* **2003**, *107*, 7337–7342.
- (33) Bouhelier, A.; Bachelot, R.; Im, J. S.; Wiederrecht, G. P.; Lerondel, G.; Kostcheev, S.; Royer, P. Electromagnetic Interactions in Plasmonic Nanoparticle Arrays. *J. Phys. Chem. B* **2005**, *109*, 3195–3198, PMID: 16851340.
- (34) Kinnan, M. K.; Chumanov, G. Plasmon Coupling in Two-Dimensional Arrays of Silver Nanoparticles: II. Effect of the Particle Size and Interparticle Distance. *J. Phys. Chem. C* **2010**, *114*, 7496–7501.
- (35) Near-, middle-, and far-field dipolar interactions in gold nanoparticle arrays. 2016; pp 97240B–97240B–8.

- (36) Jackson, J. D. *Classical Electrodynamics*, 3rd ed.; Wiley: New York, NY, 1999.
- (37) Purcell, E. M.; Pennypacker, C. R. Scattering and Absorption of Light by Nonspherical Dielectric Grains. *Astrophys. J.* **1973**, *186*, 705–714.
- (38) Draine, B. T.; Goodman, J. Beyond Clausius-Mossotti - Wave propagation on a polarizable point lattice and the discrete dipole approximation. *Astrophys. J.* **1993**, *405*, 685–697.
- (39) Yang, A.; Hoang, T. B.; Dridi, M.; Deeb, C.; Mikkelsen, M. H.; Schatz, G. C.; Odom, T. W. Real-time tunable lasing from plasmonic nanocavity arrays. *Nature Comm.* **2015**, *6*, 6939.
- (40) Qian, Z.; Guye, K. N.; Masiello, D. J.; Ginger, D. S. Dynamic Optical Switching of Polymer/Plasmonic Nanoparticle Hybrids with Sparse Loading. *The Journal of Physical Chemistry B* **2017**, *121*, 1092–1099, PMID: 28075134.
- (41) Cheng, W.; Campolongo, M. J.; Cha, J. J.; Tan, S. J.; Umbach, C. C.; Muller, D. A.; Luo, D. Free-standing nanoparticle superlattice sheets controlled by DNA. *Nature Materials* **2009**, *8*, 519–525.
- (42) Kuzyk, A.; Urban, M. J.; Idili, A.; Ricci, F.; Liu, N. Selective control of reconfigurable chiral plasmonic metamolecules. *Science Advances* **2017**, *3*.

Graphical TOC Entry

